energies

MDPI

Communication

Investigation on the Origin of Sluggish Anionic Redox Kinetics in Cation-Disordered Cathode

Qi Liang [1], Peirong Li [1], Yue Zhao [1], Supeng Chen [1], Jixiang Yin [1], Yingchun Lyu [2], Qiang Li [1,*] and Qinghao Li [1,*]

[1] College of Physics, Center for Marine Observation and Communications, Qingdao University, Qingdao 266071, China
[2] Materials Genome Institute, Shanghai University, Shanghai 200444, China
* Correspondence: liqiang@qdu.edu.cn (Q.L.); qhli@qdu.edu.cn (Q.L.)

Abstract: Cation-disordered rock salt (DRX) cathodes exhibit high specific capacity due to the simultaneous use of anionic and cationic redox reactions. However, DRX systems face severe challenges that limit their practical applications; a most important challenge is their poor rate performance. In this work, the structure and morphology of $Li_{1.17}Ti_{0.58}Ni_{0.25}O_2$ (LTNO) were characterized by X-ray diffractometry (XRD), scanning electron microscopy (SEM), transmission electron microscopy (TEM), etc. In combination with various electrochemical characterizations, we found that the sluggish kinetics of anionic redox within LTNO can be the key reason for the inferior rate performance. By sample relaxation at moderate temperature and X-ray absorption near edge structure (XANES), the ligand-to-metal charge transfer process is verified to occur between O and Ni and exhibits a prolonged characteristic time of 113.8 min. This time-consuming charge transfer process is verified to be the very fundamental origin of the slow kinetics of oxygen oxidation and reduction. This claim is further supported by the galvanostatic intermittent titration technique (GITT) at different temperatures. These findings provide essential guidance for understanding and further optimizing cathodes with anion redox reactions not only in the context of DRX cathodes but also conventional Li-rich cathodes.

Keywords: lithium-ion batteries; cation-disordered cathode; anionic redox reaction; sluggish kinetics

check for updates

Citation: Liang, Q.; Li, P.; Zhao, Y.; Chen, S.; Yin, J.; Lyu, Y.; Li, Q.; Li, Q. Investigation on the Origin of Sluggish Anionic Redox Kinetics in Cation-Disordered Cathode. *Energies* **2023**, *16*, 6740. https://doi.org/10.3390/en16186740

Academic Editor: Jin-Soo Park

Received: 11 August 2023
Revised: 15 September 2023
Accepted: 19 September 2023
Published: 21 September 2023

Copyright: © 2023 by the authors. Licensee MDPI, Basel, Switzerland. This article is an open access article distributed under the terms and conditions of the Creative Commons Attribution (CC BY) license (https://creativecommons.org/licenses/by/4.0/).

1. Introduction

Lithium-ion batteries (LIBs) form the foundation for the rapid development of energy storage applications, including portable electronics, electric vehicles, and grid-scale energy storage [1,2]. However, conventional cathodes based on transition metal (TM) redox reactions are reaching their theoretical capacity limit and becoming inadequate to meet the growing market demand. In past years, Li-rich materials utilizing both cationic redox and anionic redox reactions (ARR) have attracted wide attention [3–6]. In such materials, excessive Li offers the ability to extract electrons from non-bonding O 2p states, thus almost doubling their capacity. The extraordinary capacity beyond conventional TM redox schemes makes Li-rich material a most promising cathode candidate for the next generation of LIBs. The development of advanced technology makes it possible to understand this proposition more deeply [7–10]. To better understand the characteristics of ARR and obtain cathodes with better electrochemical performance, a variety of Li-rich materials have been designed.

Among various Li-rich cathodes, cation-disordered rock salt (DRX) cathodes show unique advantages because of their structural characteristics [11]. Unlike Li-rich NCM with layered structures, in DRX cathodes, O anions are located in the 4b sites in the $Fm\bar{3}m$ space group, while Li and TM cations are completely randomly located in the 4a sites. Traditionally, DRX cathodes are not considered to be electrochemically active due to the disordered cation distribution that hinders the Li^+ transport channel [12]. However,

Ceder and his collaborators showed that DRX cathodes containing excess Li (at least 10%) exhibit good electrochemical performance. This phenomenon can be explained by percolation theory, in which excess Li can form enough 0-TM channels to construct a Li-ion transport network [13]. The stable three-dimensional structure of DRX cathodes avoids the detrimental structural changes that often occur in Li-rich NCM with two-dimensional layered structures, such as stacking faults and TM migration to the Li layer upon deep cycle [14–17]. On the other hand, DRX cathodes also eliminate the dependence on elements that are beneficial to the layered structure such as Co and Ni. Currently, reported DRX cathodes are composed of d^0 metal (e.g., Nb^{5+}, Ti^{4+}, Zr^{4+}, Ta^{5+}, W^{6+}, Mo^{6+}, etc.) responsible for stabilizing the structure and TM (Mn, Fe, Ni, Cr, Co, etc.) with redox activity responsible for providing capacity [12,14].

Despite their high capacity, DRX cathodes face a series of problems that hinder their further application; one of the most significant challenges is their inferior rate performance [11,18]. This is a common problem in various batteries and is mainly affected by the Li^+ diffusion barrier, electrode conductivity, reaction kinetics, etc. [19]. The rate performance of batteries can be improved by materials design, such as designing 1D nanomaterials or porous structures to shorten the Na^+ transport path [20,21], doping foreign atoms to improve electronic conductivity [22], and using appropriate catalysts to promote reaction kinetics [23]. At the same time, supercapacitors with special non-diffusion storage mechanisms have unique advantages in rate performance [24]. For cathodes with ARR activity, the sluggish kinetics of anion redox is usually considered to be one of the main reasons for their inferior rate performance [25], but there are relatively few studies on the detailed and fundamental origin. Tarascon and his collaborators first pointed out the slow kinetics of the anion redox process in $Li_2Ru_{0.75}Sn_{0.25}O_3$ via in situ electron paramagnetic resonance (EPR) [26]. Li et al. discovered that coupling oxygen redox with fast Co redox can enhance the redox kinetics of oxygen [27]. Generally speaking, the ARR process is closely related to TM migration. Ku et al. found that TM migration profoundly affects the diffusion kinetics of Li in $Li_{1.2}Ni_{0.4}Mn_{0.4}O_2$ [28]. Wang et al. found that different oxygen-stacking sequences in $Na_{0.6}Mn_{0.7}Mg_{0.3}O_2$ can realize discrepant anionic redox chemistry and, thus, affect kinetics [29]. There is no doubt that the slow ARR process has a profound impact on the rate capability of Li-rich cathodes; however, it is still unclear how ARR leads to sluggish kinetics and the study of this effect on a time scale is missing. Therefore, it is difficult to fundamentally solve the poor rate performance of Li-rich cathodes, and material optimization can only be partly improved from a materials engineering viewpoint [30].

In this work, we synthesized a cation-disordered Li-rich rock salt $Li_{1.17}Ti_{0.58}Ni_{0.25}O_2$ (LTNO) by the sol–gel method and characterized its structure and electrochemistry performance by XRD, SEM, TEM, XPS, and electrochemical methods. The LTNO cathode exhibits a high specific capacity of nearly 230 mAh/g at 0.1C; however, it only exhibits a capacity of 54 mAh/g at 3C. Through the galvanostatic intermittent titration technique (GITT) and charge–discharge at different rates, we found that the kinetic performance in the anionic redox region was worse than that in the TM redox region. Then, XANES characterization verified that charge transfer takes place between oxygen and metal at high voltage. Detailed results prove that the charge transfer process exhibits a prolonged characterization time and is the rate-determining step in the charge compensation process. This charge transfer process is the key factor restricting the kinetics of ARR. GITT tests at different temperatures further support such a claim. Based on these results, this work provides rational guidelines for improving the kinetic response of cathodes with ARR activity, which is of great significance for practical applications.

2. Materials and Methods

2.1. Material Synthesis

All of the raw materials were of analytical grade and purchased from Aladdin. The pristine $Li_{1.17}Ti_{0.58}Ni_{0.25}O_2$ cathode material was synthesized by the sol−gel method; in detail, lithium acetate, nickel acetate, and tetrabutyl titanate were added into 100 mL

alcohol according to the stoichiometric ratio. In particular, 2% excess Li was added to compensate for the volatilization of lithium at high temperatures according to a report in the literature [31]. After mixing evenly, the mixed solution was heated and evaporated to obtain a viscous gel under vigorous stirring at 80 °C in a beaker. Then, the gel was dried in a vacuum oven at 120 °C for 24 h. The obtained dry gel was prepared as powder in a mortar and subsequently annealed at 650 °C for 12 h using a muffle furnace under an air atmosphere.

2.2. Material Characterization

The crystal structure of the $Li_{1.17}Ti_{0.58}Ni_{0.25}O_2$ cathode material was characterized by a Rigaku D/Max X-ray diffractometer (XRD) with Cu Kα radiation. The microstructures of the samples were characterized by scanning electron microscopy (SEM, JSM-6700F), transmission electron microscopy (TEM), high-resolution transmission electron microscopy (HRTEM), and selected-area electron diffraction (SAED) on a JEOL JEM-2100F microscope. The XANES experiments were carried out in transmission mode at beamline BL11B of the Shanghai Synchrotron Radiation Facility (SSRF). The Ni and Ti foils were measured for energy calibration. The XANES data were processed using the ATHENA software package version 0.9.26.

2.3. Electrochemical Measurements

The working electrodes were obtained by mixing the active material (80 wt%), conductive carbon black (super P, 10 wt%), and binder (polyvinylidene fluoride (PVDF), 10 wt%). The slurry was spread on an Al current collector and then dried at 120 °C overnight in a vacuum dryer and cut into discs. The average active mass loading was about 3.5 mg/cm^2 on current collectors. The CR2032 coin cells were assembled in an argon-filled glove box (<0.01 ppm of H_2O, <0.01 ppm of O_2). Li foils were used as an anode in LIBs, and a polypropylene/polyethylene microporous film (Celgard 2400) was used as the separator. Further, 1M $LiPF_6$ in fluoroethylene carbonate (FEC)/ethyl methyl carbonate (EMC) (3:7 *v*/*v*) was used as the electrolyte. The electrochemical properties of the $Li_{1.17}Ti_{0.58}Ni_{0.25}O_2$ were measured by a land instrument in the range of 1.5 and 4.8 V vs. Li/Li^+. All electrochemical data were tested several times to ensure data repeatability.

3. Results

3.1. Structural Analysis

Figure 1 shows the XRD pattern of LTNO materials prepared by the sol–gel method, which is consistent with a report in the literature [31,32]. The diffraction peaks at 37.6°, 43.8°, 63.5°, and 76.3° can be attributed to the structure of the $Fm\bar{3}m$ space group (PDF#74-2257), and no other peaks are observed. The XRD result indicates that a material with typical rock salt structure was successfully synthesized. The nanoparticle geometry demonstrates large surface area, which can improve the Li^+ diffusion coefficient [33]. HRTEM and SEAD (Figure 2b,c) provide additional evidence for the structural characteristics of LTNO. HRTEM images display clear and continuous lattice fringes with a spacing of 0.21 nm, matching well with the (200) plane in the $Fm\bar{3}m$ space group. The SAED pattern exhibits diffraction rings of LTNO, which can be accurately indexed to the cubic $Fm\bar{3}m$ phase of the cation-disordered rock salt structure [34]. These results agree well with the XRD pattern in Figure 1. All these structural characterizations confirm that a $Li_{1.17}Ti_{0.58}Ni_{0.25}O_2$ DRX cathode is successfully synthesized. The structural diagram of LTNO is shown in Figure 1. Oxygen atoms are tightly packed in an O_3-stacking manner to form a structural framework; all cations (Li, Ti, and Ni) are randomly distributed in the octahedral sites of the oxygen sub-lattice [31,34].

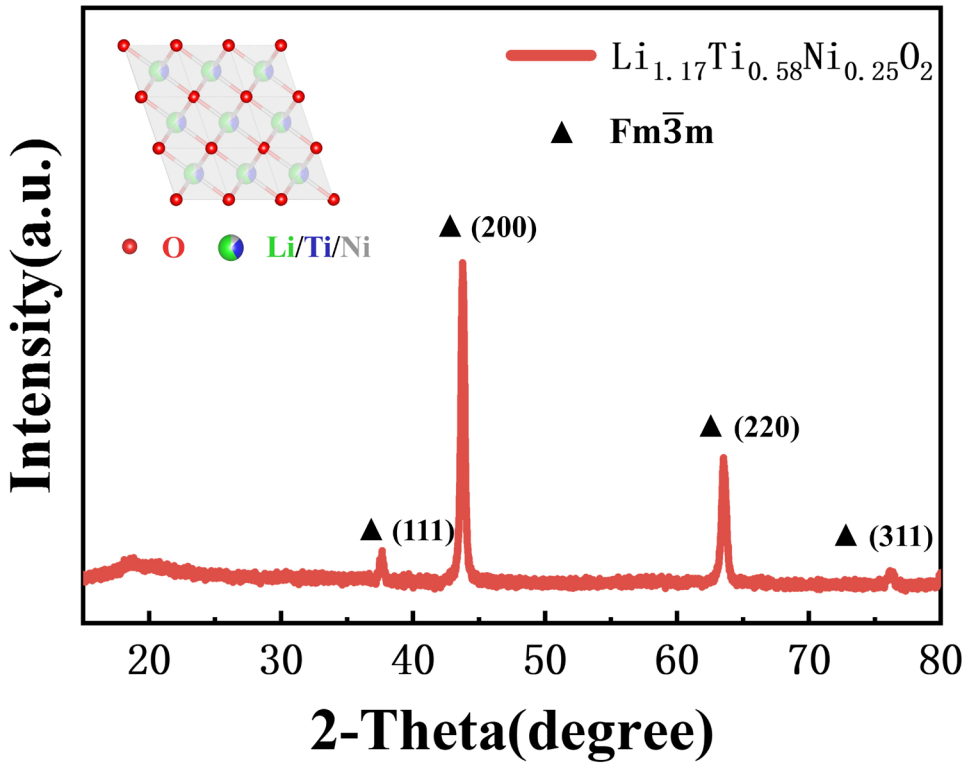

Figure 1. The XRD patterns of $Li_{1.17}Ti_{0.58}Ni_{0.25}O_2$: the inset shows the cation-disordered rock salt structure.

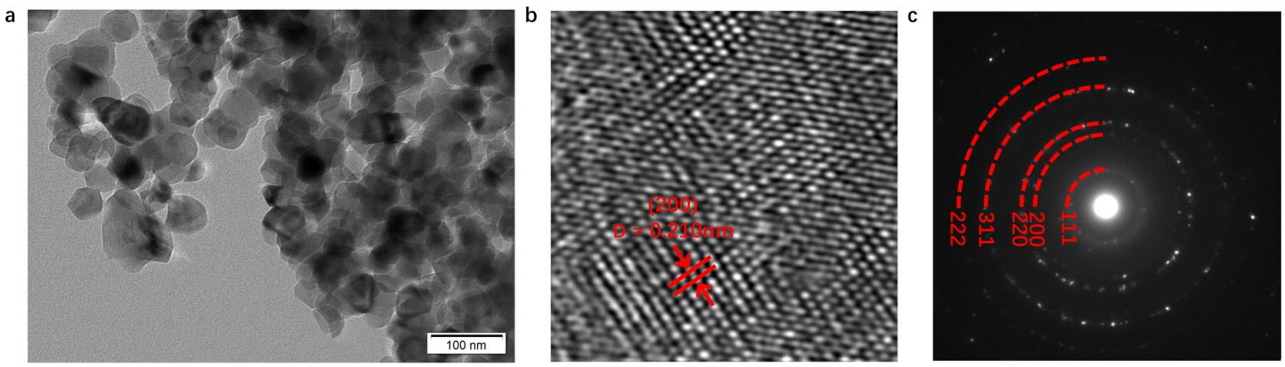

Figure 2. The structure and morphology information of $Li_{1.17}Ti_{0.58}Ni_{0.25}O_2$. (**a**) TEM result of ultrasonically dispersed LTNO, HR-TEM image, (**b**) and the selected-area electron diffraction (SAED) (**c**) of LTNO.

3.2. Electrochemical Performance Analysis

The rate capability of LTNO at 0.1C, 0.2C, 0.5C, 1C, and 3C (1C = 200 mAh/g) is shown in Figure 3a; the voltage range is 1.5 to 4.8 V and the LTNO cathode exhibits discharge capacities of 230 (±8), 189 (±7), 156 (±11), 123 (±7), and 54 (±3) mAh/g, respectively. The error between the test data is about 6.5%. Notably, the result shows that the discharge capacity of LTNO cathode decreases significantly with an increase in current density. When the rate reaches 3C, the capacity of all test samples is only 23.5% of that at 0.1C. This indicates that LTNO's exertion of its high-capacity characteristics is hindered under high current density. To further investigate the poor rate performance of LTNO, GITT was carried out to study the kinetic differences of LTNO at different stages of charge, with pulse time = 10 min and relaxation time = 30 min at 0.1C. The results are shown in Figure 3b;

the ARR and TM redox regions are highlighted in red and green shadow. Li^+ diffusion coefficients (D_{Li^+}) were calculated according to Equation (1).

$$D_{Li^+} = \frac{4}{\pi\tau}\left(\frac{m_B V_M}{M_B S}\right)^2\left(\frac{\Delta E_s}{\Delta E_\tau}\right)^2 \quad (1)$$

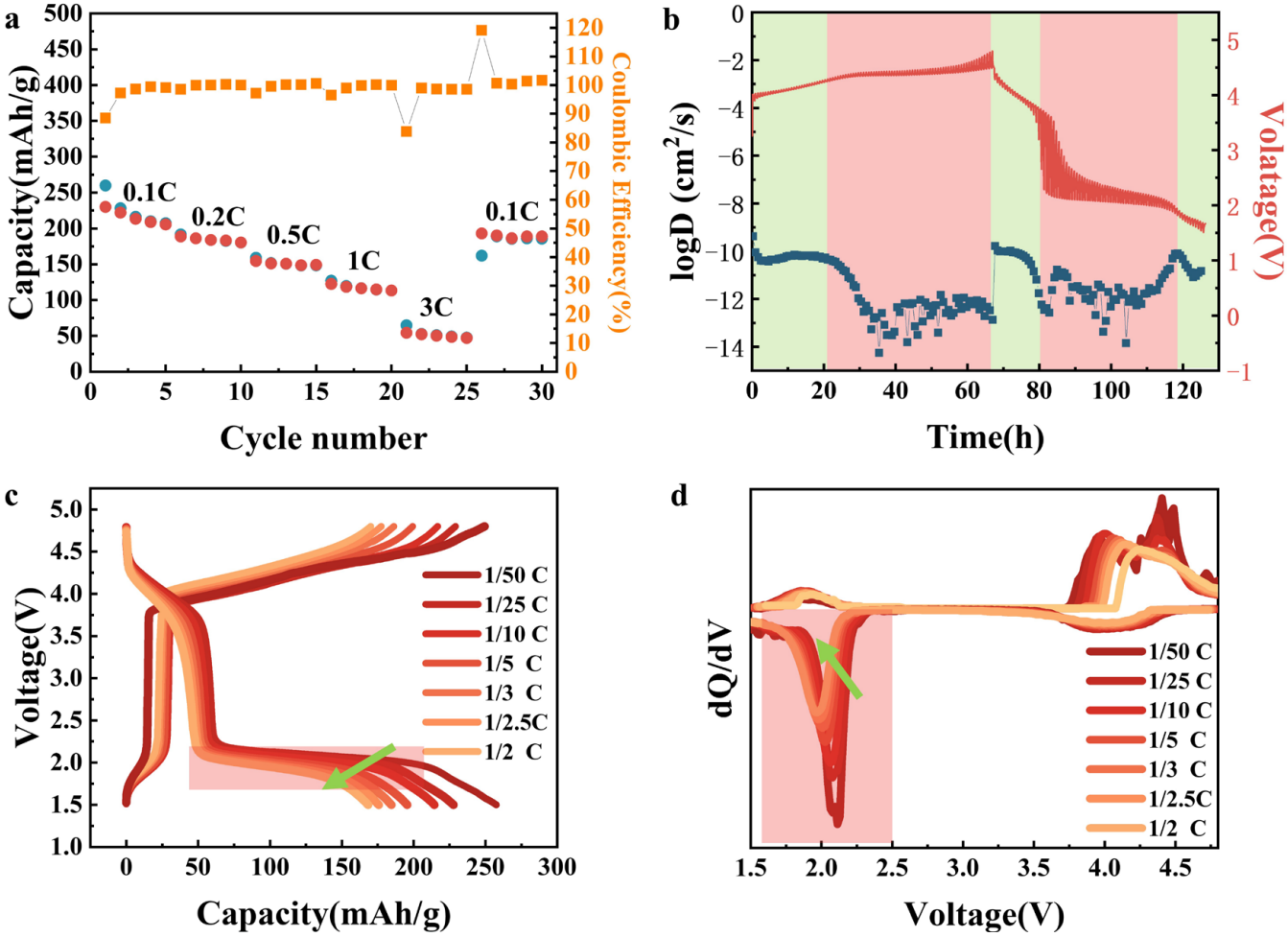

Figure 3. (**a**) Rate performance of LTNO. Blue, red and orange dots represent the charge capacity, discharge capacity and coulombic efficiency, respectively. (**b**) GITT measurement performed on the first cycle of LTNO, the GITT curve is represented by red curve and Li^+ diffusion coefficient is represented by blue dots. (**c**) After activation at 0.1C, the charge–discharge curves of LTNO from 1/50C–1/2C and (**d**) corresponding dQ/dV profile. The redox intervals of O and Ni are represented by red shadow and green shadow. The arrows indicates that the discharge voltage moves to the low voltage.

In Equation (1), τ is the constant current pulse time, ΔE_s is the total potential change, and ΔE_τ is the steady-stage potential change, as shown in Figure S3. V_M, M_B, m_B, and S stand for the molar volume, molar mass of the active material, mass of the active material, and surface area of the electrode [35]. The result shows that the diffusion coefficient of Li^+ decreases sharply from the Ni redox range to the O redox range; the difference between them is two-to-three orders of magnitude. The phenomenon that the redox kinetics of TM is much better than that of O is also widely observed in other cathodes with ARR [36]. We further conducted charge and discharge tests on LTNO materials at different rates, ranging from 1/50C to 1/2C, as shown in Figure 3c. During the discharge process, we plotted the capacity corresponding to O and Ni reduction plateaus (Figure S2), and it was observed that as the rate increased from 1/50C to 1/2C, the capacity decay of O redox (41%) was

more pronounced compared to that of Ni redox (20%). This indicates that the high specific capacity of ARR for the LTNO cathode makes it difficult for it to be fully released under high-current-density charging and discharging. Furthermore, the differential capacity (dQ/dV) curves (Figure 3d) demonstrate a decrease in the O reduction potential from 2.1 V at 1/50C to 1.95 V at 1/2C, along with a sharp decline in peak intensity, which indicates that there is a large voltage polarization in the redox range of O. In contrast, the reduction peak of Ni remains nearly unchanged, except for a slight decrease in intensity. All the results in Figure 3 demonstrate that ARR has more sluggish reaction kinetics compared to redox on nickel. The slow kinetics of ARR is the core factor limiting the rate performance of LTNO. This conclusion is also consistent with other ARR-active materials, such as $Li_{1.2}Ni_{0.13}Co_{0.13}Mn_{0.54}O_2$ and $Na_{0.6}Li_{0.2}Mn_{0.8}O_2$ [37,38].

3.3. Charge Transfer between Transition Metal and Oxygen

To uncover the underlying origin of sluggish kinetics, it is necessary to investigate the detailed charge compensation process of ARR. Tarascon and his collaborators proposed the reductive coupling scheme to clarify ARR activation in Li-rich cathodes [39]. In a recent work, they further verified the LMCT (ligand-to-metal charge transfer) procedure in LTNO, indicating that ARR operates with coordinated TM as a mediator [31,40]. Specifically, Ni^{2+} first loses electrons and is oxidized to $Ni^{3+/4+}$, and in the subsequent process, O^{2-} compensates electrons to $Ni^{3+/4+}$, so that $Ni^{3+/4+}$ is reduced back to Ni^{2+}. Note that this charge transfer process could be a significant factor impeding the kinetics of oxygen redox.

To validate the correlation between LMCT and ARR kinetics, here, the LTNO cathodes at a 4.8 V charged state are maintained at the moderate heating temperature of 100 °C with varying durations from 0 s to 8 h. XANES is then utilized to probe the valence state evolution of LTNO against heating duration. In Ni K-edge XANES, depicted in Figure 4a, a noticeable absorption edge shift to higher energy can be found from a pristine state to a 4.8 V charged (duration 0 s) state. Upon maintaining at 100 °C, Ni K-edge XANES demonstrates a gradual but obvious absorption edge shift to lower energy with increasing duration (enlarged edge shift in Figure 4c). These results indicate that nickel undergoes oxidation to a higher valence state (+3/+4) during charge but undergoes gradual Ni reduction upon relaxation. On the other hand, Ti K-edge XANES does not exhibit significant changes, suggesting that the valence state of titanium remains relatively stable throughout the charging process, as shown in Figure 4b. The absorption edge also remains nearly unchanged during heating, indicating the stable valence state of titanium. These results verify the LMCT behavior of the LTNO cathode, and the process only occurs from O to Ni while Ti remains unchanged. To further demonstrate the detailed LMCT procedure, the Ni K-edge absorption energy is plotted against duration time, as shown Figure 4d. The Ni K-edge absorption edge demonstrates a dramatic energy shift within the span of 0 s to 15 min, followed by a gradual energy shift within the span of 15 min to 500 min. Such a behavior can be well fitted within an exponential decay function according to Equation (2):

$$y = a \cdot e^{-\frac{x}{t}} + y_0 \tag{2}$$

where a = 0.28, y_0 = 8345.31, and the obtained characteristic time is long as t = 113.8 min. Such a time-consuming procedure indicates that LMCT is the key player restricting the rapid gain and loss of electrons for oxygen, i.e., the sluggish kinetics.

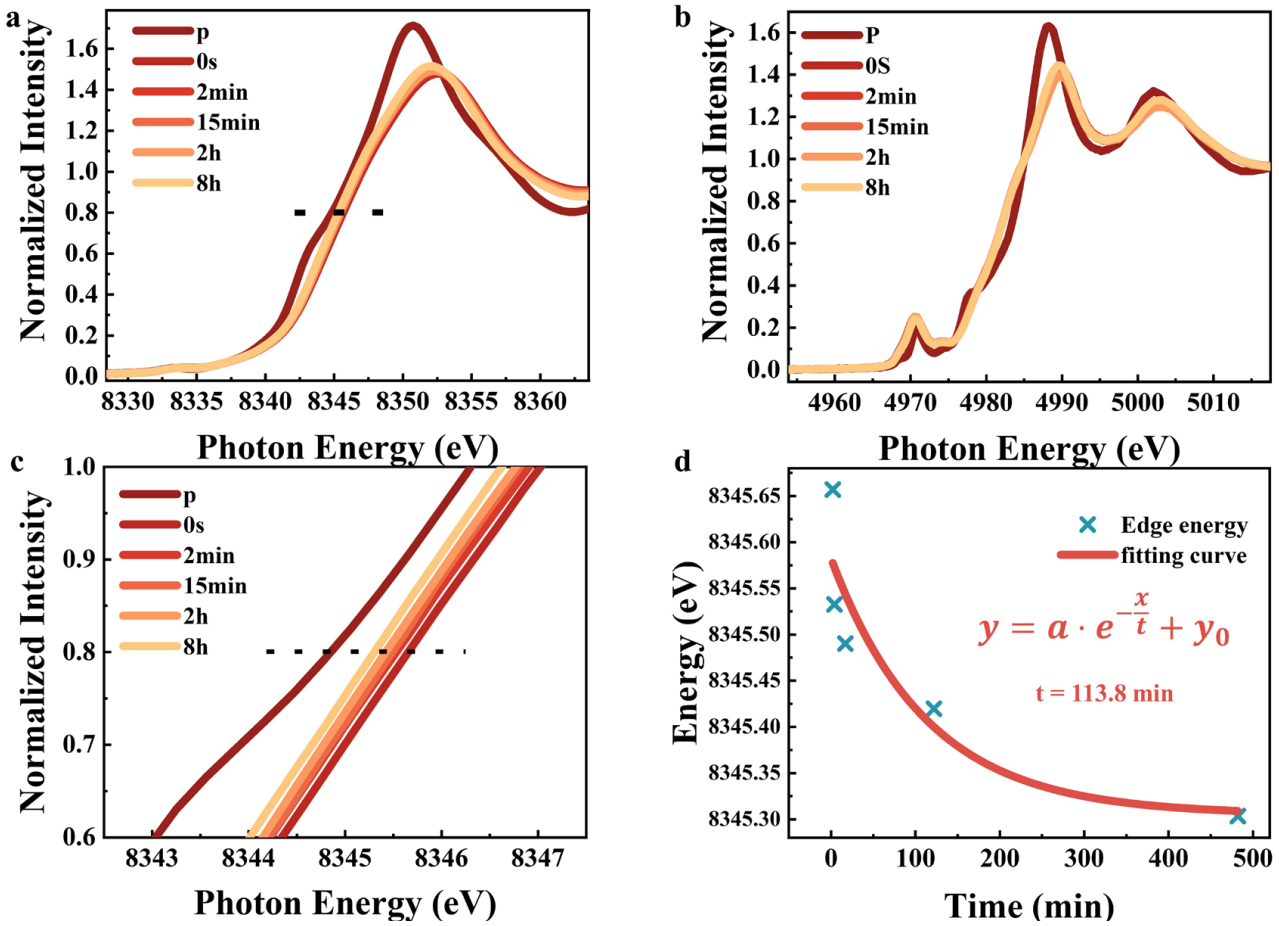

Figure 4. XANES results of (**a**) Ni K-edge and (**c**) the enlarged image of the green box; (**b**) XANES results of Ti K-edge. (**d**) The absorption edge energy of Ni K-edge in different states is plotted on the energy–time coordinate axes. The dashed line indicates the energy position of the leading edge (at a normalized absorption position of 0.8).

3.4. Kinetic Analysis

To further clarify the sluggish kinetics of ARR, we conducted GITT tests on LTNO at 25 °C and 50 °C. The GITT results at 25 °C are presented in Figure 5a,c; the results at 50 °C are shown in Figure 5b,d. The variation in the calculated Li diffusion coefficient is illustrated in Figure 5e against voltage. At the Ni redox potential range of 3.0~4.3 V, the Li diffusion coefficient at 50 °C is close to that at 25 °C, indicating that the increase in temperature from 25 °C to 50 °C has little effect on the kinetics of the Ni redox range in LTNO. As for the oxygen redox potential, ranging from 4.3~4.8 V, the Li diffusion coefficient is greatly increased at 50 °C compared with 25 °C. The onset voltage for Li diffusion coefficient increase also shifts from 4.45 V to 4.35 V. Meanwhile, it can be found that the difference between the Li diffusion coefficient in the O redox range and the Ni redox range is reduced to one-to-two orders of magnitude at 50 °C (two–three orders of magnitude at 25 °C). This contrast indicates that elevating temperature may well mitigate the energy barrier between Ni 3d and O 2p states and facilitate/accelerate the LMCT process, making it easier for oxygen to transfer electrons to nickel, thereby promoting oxygen redox kinetics. These test results further confirm the above notion that sluggish ARR kinetics arise from the LMCT process.

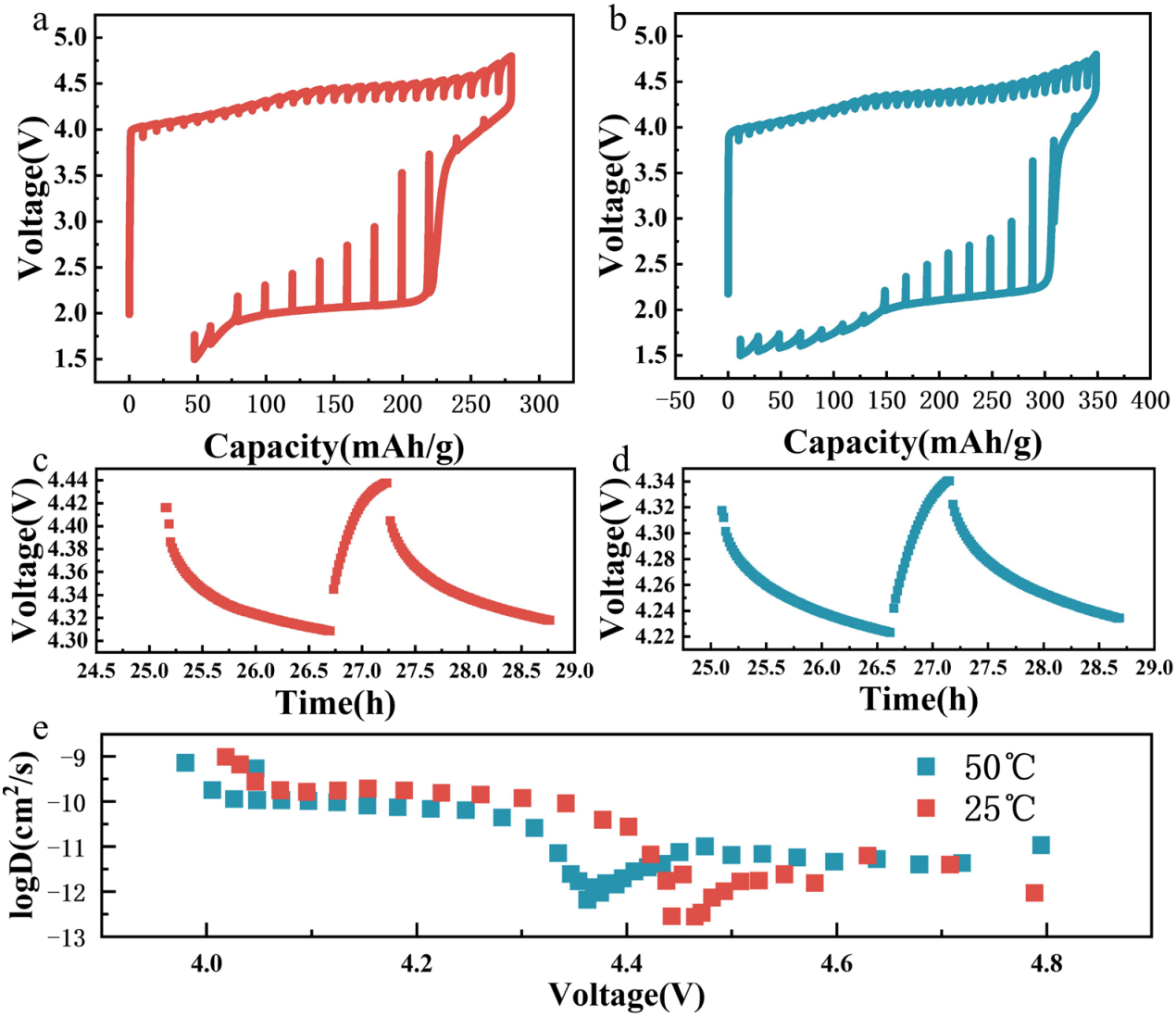

Figure 5. GITT test results at different temperatures: (**a**) 25 °C and (**b**) 50 °C and corresponding single pulse (**c**,**d**). (**e**) the variation in diffusion coefficient of Li^+ ions against voltage during the charging process.

4. Discussion

Note that the kinetic response of LIBs is a significant factor in practical applications, particularly in electric vehicles and fast-charging scenarios. Li-rich materials, comprising a most promising cathode candidate, suffer poor rate performance at high current density [25]. In addition, sluggish kinetics has been shown to have an effect on the voltage hysteresis of cathodes with ARR [41]. Such sluggish kinetics is widely attributed to ARR activation. Although the fundamental mechanism of ARR has been clarified by several schemes, including the reduction coupling model [39], local Li–O–Li model [42], and trapped molecular O_2 model [43], most ARR investigation focuses on verifying O involvement and decay mode in charge compensation [9,44,45], while the detailed origin of sluggish kinetics in ARR is missing. To uncover the kinetic response, investigation into the dynamic activity of ARR within time scales is very necessary, but such research has long been neglected until very recently [31].

In our LTNO system, it is verified that LMCT occurs between Ni and O at high voltage, and such a process exhibits a long characteristic time of 113.8 min. Note that when we use 0.1C for charge and discharge, the whole cycle is long as 20 h. Once switching to a high rate cycling like 3C, the cycle time is 20 min, which is shorter than the characteristic time

of LMCT. In addition, the atmosphere was 100 °C which may well accelerate the LMCT procedure. For practical operations at room temperature, the characteristic time may be even longer, i.e., practical LMCT can be even more sluggish. It is reasonable to expect that LMCT is the very fundamental origin and rate-determining step for the sluggish kinetics of ARR. Hence, by tuning the detailed LMCT procedure, the ARR rate performance can be modulated. Considering that such LMCT is element-selective, in this LTNO case from O to Ni, tuning energy barriers via foreign atom doping and structure design will be a promising strategy to improve rate performance, which is well supported by previous works [46–48].

More importantly, the identification of LMCT as the rate-determining factor may not be limited to DRX systems but may also work in other ARR-active cathodes. Based on previous research, the ARR activity demonstrates similar properties among various cathode systems including Li- and Na-based cathodes [49]. Sluggish kinetics, voltage hysteresis, and voltage decay are common hinderances for all these ARR-active cathode families [5]. The sluggish kinetics of LMCT verified here also provides valuable guidelines for the rational design and optimization of other ARR-active cathodes. Mitigating the energy barrier between TM and O and accelerating the LMCT procedure may well help overcome the kinetic hindrance of ARR. Increasing the battery operating temperature could be one effective method, which has been verified in previous research [50]. But elevated temperature also accelerates other battery decay modes, which is not practically accessible [51]. Modulating the LMCT-active TM element by foreign element substitution or local structure modulation may also be an effective method [27]. In such cases, high-throughput theoretical investigation may well accelerate the screening and selection of proper TM elements [52]. Above all, manipulating the LMCT procedure is the fundamental strategy toward optimizing the rate performance of ARR-active cathodes.

5. Conclusions

In this work, we synthesized LTNO materials using the sol–gel method. Combined with XRD, SEM, TEM, etc., LTNO is verified to crystallize in a rock salt structure ($Fm\bar{3}m$ space group) and presents as nanoparticles. The charge compensation is realized by Ni redox at low voltage and ARR at high voltage. GITT, rate performance, and charge–discharge tests at different rates further validate the poor rate performance of LTNO, which mostly comes from the slow kinetics of ARR. Based on delithiated LTNO relaxation and XANES characterization, the charge transfer from ligand O to coordinated Ni is verified experimentally, i.e., LMCT. The LMCT procedure demonstrates sluggish kinetics with a characterization time long as 113.8 min. GITT tests at different temperatures further support that the LMCT procedure is the ringleader of sluggish ARR kinetics. Based on these findings, rational guidelines can be proposed to optimize rate performance by regulating the LMCT process. Mitigating the energy barrier and accelerating the dynamic response of LMCT by structure design or by replacing mediate Ni are promising strategies, while detailed structure and element selection still needs further investigations. Overall, our work provides new insights into advancing the practical application of ARR-active materials, not only in DRX cathodes but also in other materials with ARR capacity.

Supplementary Materials: The following supporting information can be downloaded at: https://www.mdpi.com/article/10.3390/en16186740/s1. Figure S1: The Energy-Dispersive X-ray Spectroscopy (EDX) element diagram of LTNO cathode. Figure S2: Electrochemical properties of $Li_{1.17}Ti_{0.58}Ni_{0.25}O_2$. Figure S3: GITT partial enlargement curves. Figure S4: The capacity contribution of Ni and O at different rates. Figure S5: The cyclic performance of $Li_{1.17}Ti_{0.58}Ni_{0.25}O_2$ at 0.5C.

Author Contributions: Conceptualization, Q.L. (Qinghao Li); methodology, Q.L. (Qi Liang); investigation, Q.L. (Qi Liang) and P.L.; formal analysis, Y.Z., S.C. and J.Y.; writing—original draft preparation, Q.L. (Qi Liang); writing—review and editing, Y.L., Q.L. (Qinghao Li), Y.Z. and Q.L. (Qiang Li); supervision, Y.L., Q.L. (Qiang Li) and Q.L. (Qinghao Li); funding acquisition, Q.L. (Qinghao Li); project administration, Q.L. (Qiang Li). All authors have read and agreed to the published version of the manuscript.

Funding: This research was funded by National Science Foundation of China (No. 22179066), the Shandong Provincial Natural Science Foundation (ZR202103010205), and the Startup Foundation for Advanced Talents in Qingdao University (DC2000005106).

Data Availability Statement: Data related to this publication are available upon request from the corresponding author.

Acknowledgments: The authors acknowledge the support from beamline BL11B at SSRF during the experiments.

Conflicts of Interest: The authors declare no conflict of interest.

References

1. Wu, F.; Maier, J.; Yu, Y. Guidelines and trends for next-generation rechargeable lithium and lithium-ion batteries. *Chem. Soc. Rev.* **2020**, *49*, 1569–1614. [CrossRef] [PubMed]
2. Gandoman, F.H.; Jaguemont, J.; Goutam, S.; Gopalakrishnan, R.; Firouz, Y.; Kalogiannis, T.; Omar, N.; Van Mierlo, J. Concept of reliability and safety assessment of lithium-ion batteries in electric vehicles: Basics, progress, and challenges. *Appl. Energy* **2019**, *251*, 113343. [CrossRef]
3. He, W.; Guo, W.B.; Wu, H.L.; Lin, L.; Liu, Q.; Han, X.; Xie, Q.S.; Liu, P.F.; Zheng, H.F.; Wang, L.S.; et al. Challenges and Recent Advances in High Capacity Li-Rich Cathode Materials for High Energy Density Lithium-Ion Batteries. *Adv. Mater.* **2021**, *33*, 2005937. [CrossRef] [PubMed]
4. Zhang, M.; Kitchaev, D.A.; Lebens-Higgins, Z.; Vinckeviciute, J.; Zuba, M.; Reeves, P.J.; Grey, C.P.; Whittingham, M.S.; Piper, L.F.J.; Van der Ven, A.; et al. Pushing the limit of 3d transition metal-based layered oxides that use both cation and anion redox for energy storage. *Nat. Rev. Mater.* **2022**, *7*, 522–540. [CrossRef]
5. Assat, G.; Tarascon, J.-M. Fundamental understanding and practical challenges of anionic redox activity in Li-ion batteries. *Nat. Energy* **2018**, *3*, 373–386. [CrossRef]
6. Jiao, S.C.; Wang, J.Y.; Hu, Y.S.; Yu, X.Q.; Li, H. High-Capacity Oxide Cathode beyond 300 mAh/g Focus Review. *Acs Energy Lett.* **2023**, *8*, 3025–3037. [CrossRef]
7. Mukai, K.; Nonaka, T.; Uyama, T.; Nishimura, Y.F. In situ X-ray Raman spectroscopy and magnetic susceptibility study on the $Li[Li_{0.15}Mn_{1.85}]O_4$ oxygen anion redox reaction. *Chem. Commun.* **2020**, *56*, 1701–1704. [CrossRef]
8. Li, Q.; Li, H.; Xia, Q.; Hu, Z.; Zhu, Y.; Yan, S.; Ge, C.; Zhang, Q.; Wang, X.; Shang, X.; et al. Extra storage capacity in transition metal oxide lithium-ion batteries revealed by in situ magnetometry. *Nat. Mater.* **2020**, *20*, 76–83. [CrossRef]
9. Li, Q.H.; Liang, Q.; Zhang, H.; Jiao, S.C.; Zhuo, Z.Q.; Wang, J.Y.; Li, Q.; Zhang, J.N.; Yu, X.Q. Unveiling the High-valence Oxygen Degradation across the Delithiated Cathode Surface. *Angew. Chem.-Int. Ed.* **2022**, *62*, e202215131. [CrossRef]
10. Zhao, C.; Li, C.; Liu, H.; Qiu, Q.; Geng, F.; Shen, M.; Tong, W.; Li, J.; Hu, B. Coexistence of (O_2)(n-) and Trapped Molecular O_2 as the Oxidized Species in P2-Type Sodium 3d Layered Oxide and Stable Interface Enabled by Highly Fluorinated Electrolyte. *J. Am. Chem. Soc.* **2021**, *143*, 18652–18664. [CrossRef]
11. Yabuuchi, N. Rational material design of Li-excess metal oxides with disordered rock salt structure. *Curr. Opin. Electrochem.* **2022**, *34*, 100978. [CrossRef]
12. Clément, R.J.; Lun, Z.; Ceder, G. Cation-disordered rocksalt transition metal oxides and oxyfluorides for high energy lithium-ion cathodes. *Energy Environ. Sci.* **2020**, *13*, 345–373. [CrossRef]
13. Lee, J.; Urban, A.; Li, X.; Su, D.; Hautier, G.; Ceder, G. Unlocking the Potential of Cation-Disordered Oxides for Rechargeable Lithium Batteries. *Science* **2014**, *343*, 519–522. [CrossRef] [PubMed]
14. Chen, D.C.; Ahn, J.; Chen, G.Y. An Overview of Cation-Disordered Lithium-Excess Rocksalt Cathodes. *Acs Energy Lett.* **2021**, *6*, 1358–1376. [CrossRef]
15. Hyun, H.; Yoon, H.; Choi, S.; Kim, J.; Kim, S.Y.; Regier, T.; Arthur, Z.; Kim, S.; Lim, J. Paradoxical role of structural degradation of nickel-rich layered oxides in capacity retention upon storage of lithium-ion batteries. *Energy Environ. Sci.* **2023**, *16*, 3968–3983. [CrossRef]
16. Li, L.; Self, E.C.; Darbar, D.; Zou, L.; Bhattacharya, I.; Wang, D.; Nanda, J.; Wang, C. Hidden Subsurface Reconstruction and Its Atomic Origins in Layered Oxide Cathodes. *Nano Lett.* **2020**, *20*, 2756–2762. [CrossRef]
17. Mu, L.; Lin, R.; Xu, R.; Han, L.; Xia, S.; Sokaras, D.; Steiner, J.D.; Weng, T.-C.; Nordlund, D.; Doeff, M.M.; et al. Oxygen Release Induced Chemomechanical Breakdown of Layered Cathode Materials. *Nano Lett.* **2018**, *18*, 3241–3249. [CrossRef]

18. McColl, K.; House, R.A.; Rees, G.J.; Squires, A.G.; Coles, S.W.; Bruce, P.G.; Morgan, B.J.; Islam, M.S. Transition metal migration and O_2 formation underpin voltage hysteresis in oxygen-redox disordered rocksalt cathodes. *Nat. Commun.* **2022**, *13*, 5275. [CrossRef]
19. He, J.; Meng, J.; Huang, Y. Challenges and recent progress in fast-charging lithium-ion battery materials. *J. Power Sources* **2023**, *570*, 232965. [CrossRef]
20. Jin, T.; Han, Q.; Wang, Y.; Jiao, L. 1D Nanomaterials: Design, Synthesis, and Applications in Sodium-Ion Batteries. *Small* **2018**, *14*, 1703086. [CrossRef]
21. Balasankar, A.; Arthiya, S.; Ramasundaram, S.; Sumathi, P.; Arokiyaraj, S.; Oh, T.; Aruchamy, K.; Sriram, G.; Kurkuri, M. Recent Advances in the Preparation and Performance of Porous Titanium-Based Anode Materials for Sodium-Ion Batteries. *Energies* **2022**, *15*, 9495. [CrossRef]
22. Aruchamy, K.; Balasankar, A.; Ramasundaram, S.; Oh, T.H. Recent Design and Synthesis Strategies for High-Performance Supercapacitors Utilizing $ZnCo_2O_4$-Based Electrode Materials. *Energies* **2023**, *16*, 5604. [CrossRef]
23. Tang, X.; Xu, Z.; Sun, Z.; Zhou, J.; Wu, X.; Lin, H.; Rong, J.; Zhuo, S.; Li, F. Factors of Kinetics Processes in Lithium–Sulfur Reactions. *Energy Technol.* **2019**, *7*, 1900574. [CrossRef]
24. Das, A.; Raj, B.; Mohapatra, M.; Andersen, S.M.; Basu, S. Performance and future directions of transition metal sulfide-based electrode materials towards supercapacitor/supercapattery. *WIREs Energy Environ.* **2022**, *11*, e414. [CrossRef]
25. Zhao, S.; Guo, Z.; Yan, K.; Wan, S.; He, F.; Sun, B.; Wang, G. Towards high-energy-density lithium-ion batteries: Strategies for developing high-capacity lithium-rich cathode materials. *Energy Storage Mater.* **2021**, *34*, 716–734. [CrossRef]
26. Sathiya, M.; Leriche, J.B.; Salager, E.; Gourier, D.; Tarascon, J.M.; Vezin, H. Electron paramagnetic resonance imaging for real-time monitoring of Li-ion batteries. *Nat. Commun.* **2015**, *6*, 6276. [CrossRef]
27. Li, N.; Wu, J.; Hwang, S.; Papp, J.K.; Kan, W.H.; Zhang, L.; Zhu, C.; McCloskey, B.D.; Yang, W.; Tong, W. Enabling Facile Anionic Kinetics through Cationic Redox Mediator in Li-Rich Layered Cathodes. *ACS Energy Lett.* **2020**, *5*, 3535–3543. [CrossRef]
28. Ku, K.; Kim, B.; Jung, S.-K.; Gong, Y.; Eum, D.; Yoon, G.; Park, K.-Y.; Hong, J.; Cho, S.-P.; Kim, D.-H.; et al. A new lithium diffusion model in layered oxides based on asymmetric but reversible transition metal migration. *Energy Environ. Sci.* **2020**, *13*, 1269–1278. [CrossRef]
29. Wang, D.; Liu, Y.; Wu, Z.; Liu, Y.; Zhu, C.; Zhong, B.; Guo, X. Realizing discrepant oxygen-redox chemistry in honeycomb superlattice cathode via manipulating oxygen-stacking sequences. *Chem. Eng. J.* **2023**, *462*, 141994. [CrossRef]
30. Huang, J.; Zhong, P.; Ha, Y.; Kwon, D.-H.; Crafton, M.J.; Tian, Y.; Balasubramanian, M.; McCloskey, B.D.; Yang, W.; Ceder, G. Non-topotactic reactions enable high rate capability in Li-rich cathode materials. *Nat. Energy* **2021**, *6*, 706–714. [CrossRef]
31. Li, B.A.; Kumar, K.; Roy, I.; Morozov, A.V.; Emelyanova, O.V.; Zhang, L.T.; Koc, T.; Belin, S.; Cabana, J.; Dedryvere, R.; et al. Capturing dynamic ligand-to-metal charge transfer with a long-lived cationic intermediate for anionic redox. *Nat. Mater.* **2022**, *21*, 1165–1174. [CrossRef] [PubMed]
32. Liu, Y.; Zheng, S.; Wan, H.; Dou, A.; Chu, D.; Su, M. Synthesis and electrochemical properties of cation-disordered Li-Ni-Ti-O compounds as cathode material for lithium ion batteries. *J. Alloys Compd.* **2017**, *728*, 659–668. [CrossRef]
33. Zhang, Y.X.; Hu, A.Y.; Liu, J.; Xu, Z.R.; Mu, L.Q.; Sainio, S.; Nordlund, D.; Li, L.X.; Sun, C.J.; Xiao, X.H.; et al. Investigating Particle Size-Dependent Redox Kinetics and Charge Distribution in Disordered Rocksalt Cathodes. *Adv. Funct. Mater.* **2022**, *32*, 2110502. [CrossRef]
34. Yu, Z.; Qu, X.; Dou, A.; Su, M.; Liu, Y.; Wu, F. Synthesis and Redox Mechanism of Cation-Disordered, Rock-Salt Cathode-Material Li-Ni-Ti-Nb-O Compounds for a Li-Ion Battery. *ACS Appl. Mater. Interfaces* **2019**, *11*, 35777–35787. [CrossRef] [PubMed]
35. Tang, W.; Li, A.; Zhou, G.; Chen, Z.; Yang, Z.; Su, J.; Zhang, W. Structural Stabilization of Cation-Disordered Rock-Salt Cathode Materials: Coupling between a High-Ratio Inactive Ti^{4+} Cation and a Mn^{2+}/Mn^{4+} Two-Electron Redox Pair. *ACS Appl. Mater. Interfaces* **2022**, *14*, 38865–38874. [CrossRef] [PubMed]
36. Hwang, J.; Myeong, S.; Jin, W.; Jang, H.; Nam, G.; Yoon, M.; Kim, S.H.; Joo, S.H.; Kwak, S.K.; Kim, M.G.; et al. Excess-Li Localization Triggers Chemical Irreversibility in Li- and Mn-Rich Layered Oxides. *Adv. Mater.* **2020**, *32*, 2001944. [CrossRef] [PubMed]
37. Sun, G.; Yu, F.-D.; Zhao, C.; Yu, R.; Farnum, S.; Shao, G.; Sun, X.; Wang, Z.-B. Decoupling the Voltage Hysteresis of Li-Rich Cathodes: Electrochemical Monitoring, Modulation Anionic Redox Chemistry and Theoretical Verifying. *Adv. Funct. Mater.* **2021**, *31*, 2002643. [CrossRef]
38. House, R.A.; Rees, G.J.; McColl, K.; Marie, J.J.; Garcia-Fernandez, M.; Nag, A.; Zhou, K.J.; Cassidy, S.; Morgan, B.J.; Islam, M.S.; et al. Delocalized electron holes on oxygen in a battery cathode. *Nat. Energy* **2023**, *8*, 351–360. [CrossRef]
39. Sathiya, M.; Rousse, G.; Ramesha, K.; Laisa, C.P.; Vezin, H.; Sougrati, M.T.; Doublet, M.L.; Foix, D.; Gonbeau, D.; Walker, W.; et al. Reversible anionic redox chemistry in high-capacity layered-oxide electrodes. *Nat. Mater.* **2013**, *12*, 827–835. [CrossRef]
40. Li, B.; Sougrati, M.T.; Rousse, G.; Morozov, A.V.; Dedryvère, R.; Iadecola, A.; Senyshyn, A.; Zhang, L.; Abakumov, A.M.; Doublet, M.-L.; et al. Correlating ligand-to-metal charge transfer with voltage hysteresis in a Li-rich rock-salt compound exhibiting anionic redox. *Nat. Chem.* **2021**, *13*, 1070–1080. [CrossRef]
41. Li, B.; Assat, G.; Pearce, P.E.; Nikitina, V.A.; Iadecola, A.; Delacourt, C.; Tarascon, J.-M. Exploring the Kinetic Limitations Causing Unusual Low-Voltage Li Reinsertion in Either Layered or Tridimensional Li_2IrO_3 Cathode Materials. *Chem. Mater.* **2020**, *32*, 2133–2147. [CrossRef]

42. Seo, D.-H.; Lee, J.; Urban, A.; Malik, R.; Kang, S.; Ceder, G. The structural and chemical origin of the oxygen redox activity in layered and cation-disordered Li-excess cathode materials. *Nat. Chem.* **2016**, *8*, 692–697. [CrossRef] [PubMed]
43. House, R.A.; Rees, G.J.; Pérez-Osorio, M.A.; Marie, J.-J.; Boivin, E.; Robertson, A.W.; Nag, A.; Garcia-Fernandez, M.; Zhou, K.-J.; Bruce, P.G. First-cycle voltage hysteresis in Li-rich 3d cathodes associated with molecular O_2 trapped in the bulk. *Nat. Energy* **2020**, *5*, 777–785. [CrossRef]
44. Zhuo, Z.; Dai, K.; Wu, J.; Zhang, L.; Tamura, N.; Chuang, Y.-d.; Feng, J.; Guo, J.; Shen, Z.-x.; Liu, G.; et al. Distinct Oxygen Redox Activities in Li_2MO_3 (M = Mn, Ru, Ir). *ACS Energy Lett.* **2021**, *6*, 3417–3424. [CrossRef]
45. Wu, J.; Zhuo, Z.; Rong, X.; Dai, K.; Lebens-Higgins, Z.; Sallis, S.; Pan, F.; Piper Louis, F.J.; Liu, G.; Chuang, Y.-d.; et al. Dissociate lattice oxygen redox reactions from capacity and voltage drops of battery electrodes. *Sci. Adv.* **2020**, *6*, eaaw3871. [CrossRef]
46. Zhou, J.; Chen, Z.; Yu, G.; Ma, K.; Lian, X.; Li, S.; Shi, Q.; Wang, J.; Guo, L.; Liu, Y.; et al. Accelerating O-Redox Kinetics with Carbon Nanotubes for Stable Lithium-Rich Cathodes. *Small Methods* **2022**, *6*, e2200449. [CrossRef]
47. Yu, R.; Banis, M.N.; Wang, C.; Wu, B.; Huang, Y.; Cao, S.; Li, J.; Jamil, S.; Lin, X.; Zhao, F.; et al. Tailoring bulk Li+ ion diffusion kinetics and surface lattice oxygen activity for high-performance lithium-rich manganese-based layered oxides. *Energy Storage Mater.* **2021**, *37*, 509–520. [CrossRef]
48. Tu, W.Q.; Wang, X.S.; Tian, W.Y.; Zhou, Y.N.; Han, C.P.; Li, C.; Kang, F.Y.; Li, B.H. A green water-induced spinel heterostructure interface enabling high performance lithium and manganese rich oxides. *J. Mater. Chem. A* **2021**, *9*, 20576–20584. [CrossRef]
49. Ren, H.; Li, Y.; Ni, Q.; Bai, Y.; Zhao, H.; Wu, C. Unraveling Anionic Redox for Sodium Layered Oxide Cathodes: Breakthroughs and Perspectives. *Adv. Mater.* **2022**, *34*, e2106171. [CrossRef]
50. Lin, H.; Moreno, B.; Kucuk, K.; Zhang, S.; Aryal, S.; Li, Z.; Segre, C.U.; Rodriguez, J.; Puthusseri, D.; Cai, L.; et al. Fundamental understanding of high-capacity lithium-excess cathodes with disordered rock salt structure. *J. Mater. Sci. Technol.* **2021**, *74*, 60–68. [CrossRef]
51. Rodrigues, M.-T.F.; Babu, G.; Gullapalli, H.; Kalaga, K.; Sayed, F.N.; Kato, K.; Joyner, J.; Ajayan, P.M. A materials perspective on Li-ion batteries at extreme temperatures. *Nat. Energy* **2017**, *2*, 17108. [CrossRef]
52. Alberi, K.; Nardelli, M.B.; Zakutayev, A.; Mitas, L.; Curtarolo, S.; Jain, A.; Fornari, M.; Marzari, N.; Takeuchi, I.; Green, M.L.; et al. The 2019 materials by design roadmap. *J. Phys. D Appl. Phys.* **2019**, *52*, 013001. [CrossRef] [PubMed]

Disclaimer/Publisher's Note: The statements, opinions and data contained in all publications are solely those of the individual author(s) and contributor(s) and not of MDPI and/or the editor(s). MDPI and/or the editor(s) disclaim responsibility for any injury to people or property resulting from any ideas, methods, instructions or products referred to in the content.